Supplementary Material for:

# Effect of Stacking Interactions on the Translation of Structurally Related Bis-thiosemicarbazone Ni(II) HER Catalysts to Modified Electrode Surfaces

Alexander J. Gupta,[1⊥] Nicholas S. Vishnosky,[2⊥] Oleksandr Hietsoi,[2] Yaroslav Losovyj,[3] Jacob Strain,[2] Joshua Spurgeon,[4] Mark S. Mashuta,[2] Rahul Jain,[2]
Robert M. Buchanan,[2] Gautam Gupta,*[1] and Craig A. Grapperhaus*[2]

[1]Department of Chemical Engineering, University of Louisville, Louisville, Kentucky 40292, USA.

[2]Department of Chemistry, University of Louisville, Louisville, Kentucky 40292, USA.

[3]Department of Chemistry, Indiana University Bloomington, Bloomington, Indiana, 47405, USA.

[4]Conn Center for Renewable Energy Research, University of Louisville, Louisville, Kentucky 40292, USA.

Table of Contents

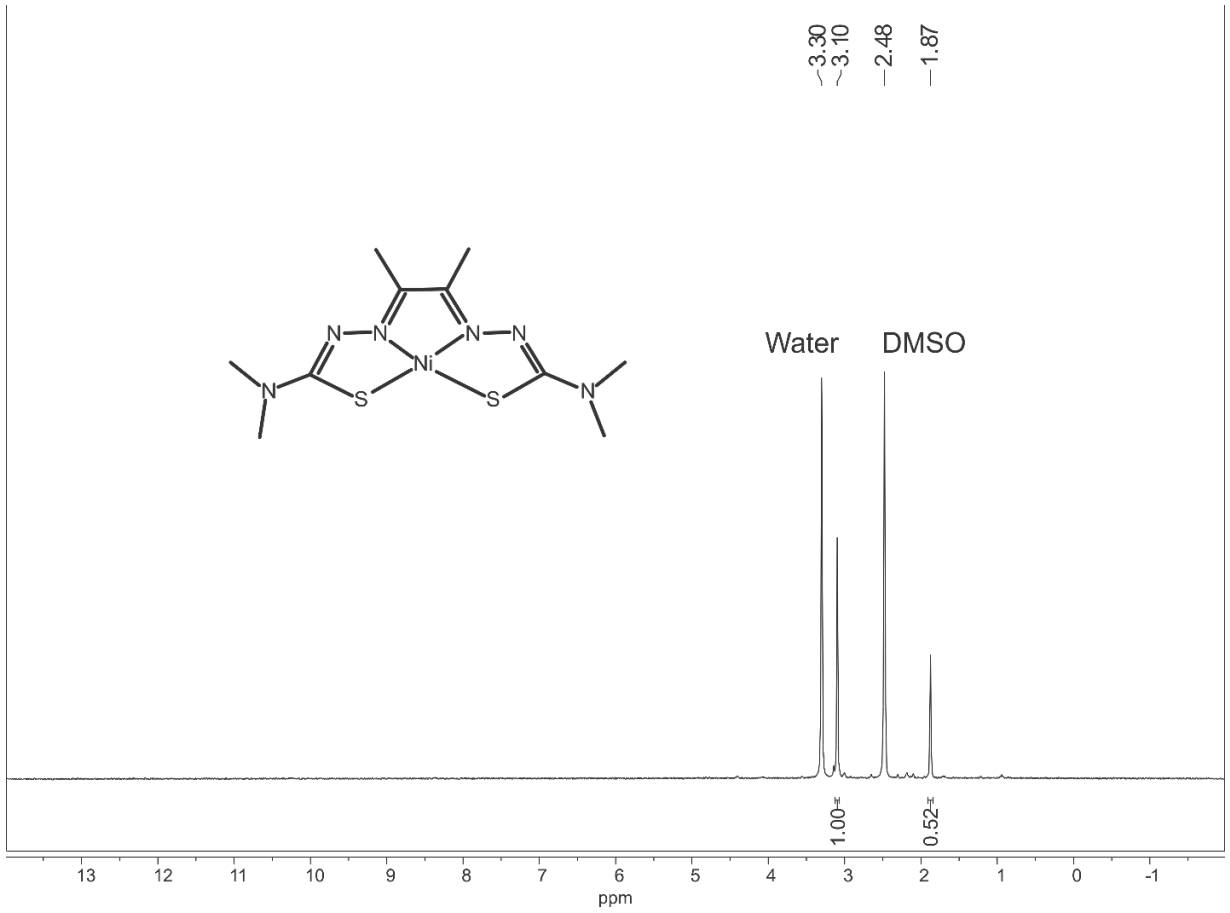


**Figure S1. $^{1}$H NMR (400 MHz) of 2 in DMSO-$d_6$.**

δ 1.87 (s, 6H) 3.10 (s, 12H)

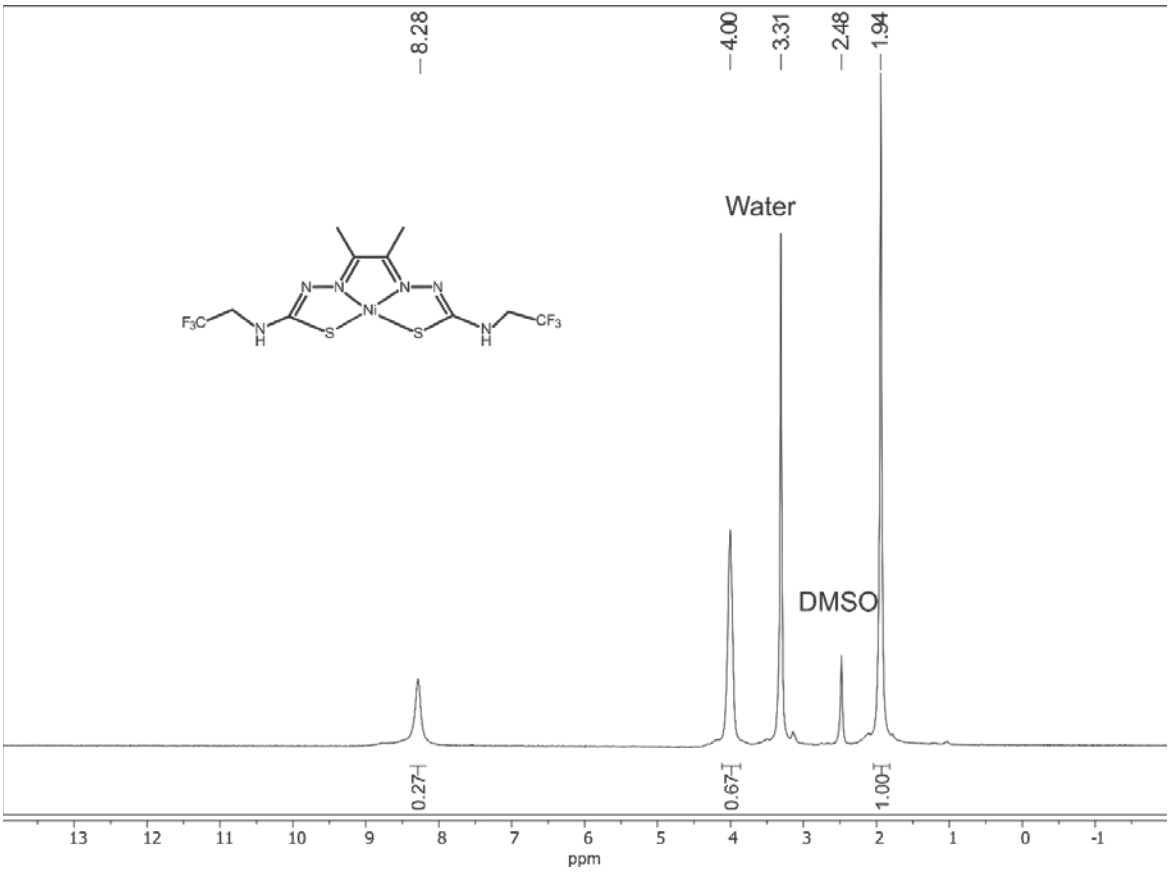


**Figure S2. $^{1}$H NMR (400 MHz) of 3 in DMSO-d$_6$.**

δ 1.94 (s, 6H) 4.00 (br, 4H) 8.28 (s, 2H)

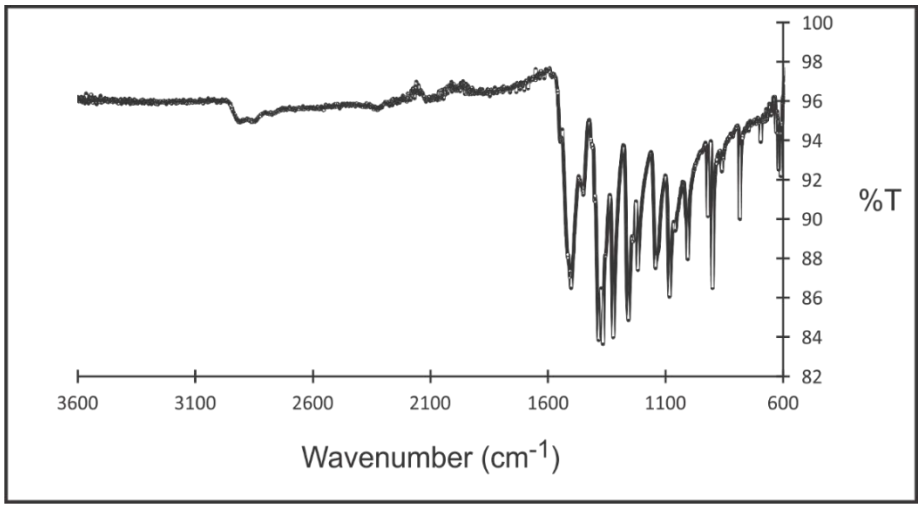


**Figure S3. FTIR of 2 as a powder (ATR).**

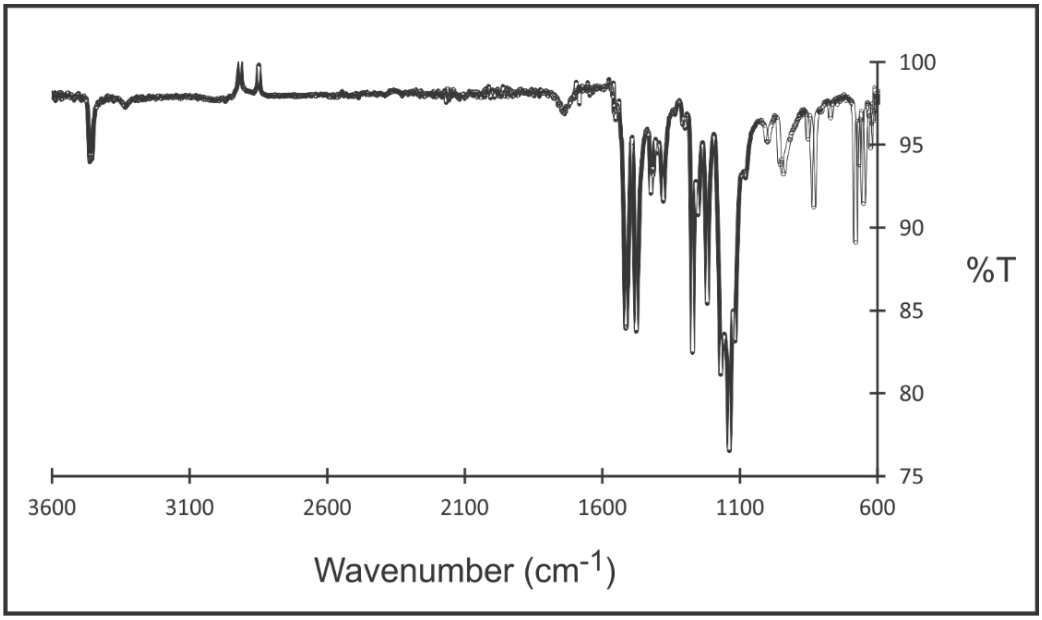


**Figure S4. FTIR of 3 as a powder (ATR).**

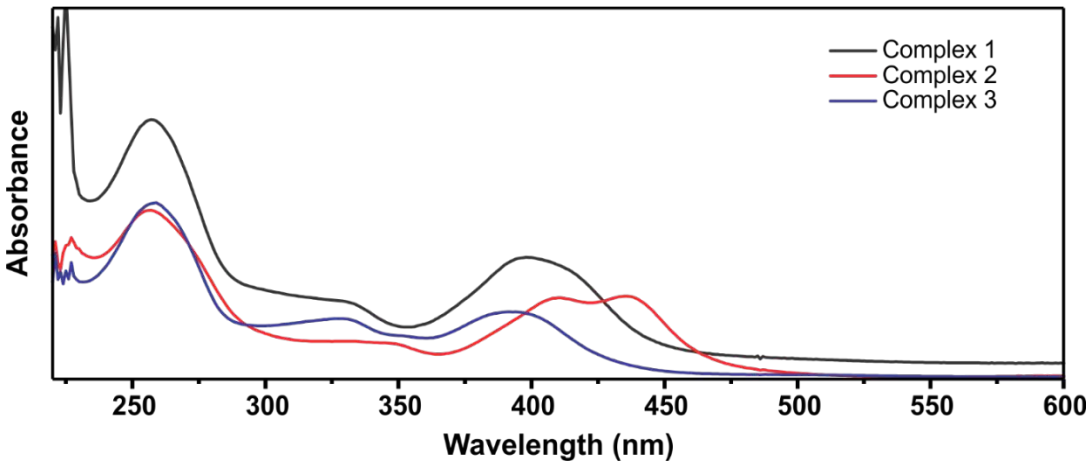


**Figure S5. UV-visible spectra of 1 – 3 in acetonitrile.**

**Table S1: Crystal data and structural refinement for Complexes 2 and 3.**

| Compound | NiATSDM (Complex **2**) | NiATSM-$F_6$ (Complex **3**) |
|---|---|---|
| Empirical formula | $C_{10}H_{18}N_6NiS_2$ | $C_{10}H_{12}F_6N_6NiS_2$ |
| Formula weight | 345.13 | 453.09 |
| Temperature (K) | 100.2(6) | 100(2) |
| Wavelength (Å) | 0.71073 | 0.71073 |
| Crystal system | Triclinic | Triclinic |
| Space group | P -1 | P -1 |
| Unit cell dimension | a = 7.33437(16) | a = 8.3598(10) |
| | b = 8.5595(2) | b = 9.4027(10) |
| | c = 11.6784 | c = 13.5112(17) |
| | α = 103.865(2) | α = 109.467 |
| | β = 98.2102(19) | β = 105.475(11) |
| | γ = 91.7205(18) | γ = 91.382(9) |
| Volume ($Å^3$) | 702.92(3) | 957.53(19) |
| Z | 2 | 2 |
| $\rho_{calcd..}$ ($Mg/m^3$) | 1.631 | 1.571 |
| Abs. coeff. ($mm^{-1}$) | 1.672 | 1.291 |
| F(000) | 360 | 456 |
| Crystal colour, habit | Orange prism | Red-brown plate |
| Crystal size ($mm^3$) | 0.40 x 0.34 x 0.18 | 0.41 x 0.08 x 0.01 |
| Θ range data collection (°) | 3.40 to 31.57 | 3.30 to 26.67 |
| Index ranges | -10≤ h ≤ 10 | -10≤ h ≤ 10 |
| | -12 ≤ k ≤12 | -11 ≤ k ≤11 |
| | -17 ≤ l ≤ 17 | -17 ≤ l ≤ 17 |
| Reflections collected | 19998 | 13904 |
| Independent reflections | 4702 [R(int) = 0.0217] | 4031 [R(int) = 0.058] |
| Completeness to θ max | 99.9 % | 99.7% |
| Absorption correction | Multiscan | Multiscan |
| Max. and min. trans. | 1.000 and 0.778 | 1.00 and 0.678 |
| Refinement method | Full-matrix least-squares on $F^2$ | Full-matrix least-squares on $F^2$ |
| Data/restraints/params | 4702/0/244 | 4031/0/288 |
| Goodness-of-fit- on $F^2$ | 1.013 | 1.074 |
| Final R indices | R1 = 0.0196 | R1 = 0.0500 |
| [I>2σ(I)][a,b] | wR2 = 0.0533 | wR2 = 0.1099 |
| R indices (all data) | R1 = 0.0211 | R1 = 0.0647 |
| | wR2 = 0.0545 | wR2 = 0.1188 |
| Largest difference peak and hole ($e·Å^3$) | 0.525 and -0.285 | 1.176 and -0.477 |

[a]$R1 = \Sigma||F_o| - |F_c||/\Sigma|F_o|$; [b] $wR2 = \{\Sigma[w(F_o^2 - F_c^2)^2]/\Sigma[w(F_o^2)^2]\}^{1/2}$; where $w = q/\sigma^2(F_o^2) + (qp)^2 + bp$. GOF = $S = \{\Sigma[w(F_o^2 - F_c^2)^2]/(n - p)\}^{1/2}$, where n is the number of reflections and p is the number of parameters refined.

| **Table S2. Selected bond distances (Å) and bond angles (°) for 1,[1] 2, and 3.** | | | |
|---|---|---|---|
| Bond distance | **1**[a] | **2** | **3** |
| Ni-N1 | 1.861(2) | 1.8528(8) | 1.854(3) |
| Ni-N3 | 1.855(2) | 1.8580(8) | 1.863(3) |
| Ni-S1 | 2.1546(6) | 2.1617(3) | 2.1542(11) |
| Ni-S2 | 2.1598(7) | 2.1576(2) | 2.1527(10) |
| S1-C5 | 1.767(3) | 1.7665(9) | 1.763(4) |
| N2-C5 | 1.315(3) | 1.3222(12) | 1.308(5) |
| N1-N2 | 1.378(3) | 1.3694(11) | 1.381(4) |
| N1-C1 | 1.303(3) | 1.3038(11) | 1.310(5) |
| C1-C3 | 1.489(4) | 1.4857(13) | 1.487(5) |
| C1-C2 | 1.470(3) | 1.4658(13) | 1.474(5) |
| N5-C5 | 1.339(3) | 1.3456(12) | 1.350(5) |
| N5-C7 | 1.449(3) | 1.4570(13) | 1.440(5) |
| Bond angle | | | |
| N1-Ni-S1 | 87.07(6) | 87.09(3) | 87.35(10) |
| N1-Ni-N3 | 83.59(9) | 83.66(4) | 83.65(13) |
| S2-Ni-S1 | 101.81(3) | 102.019(10) | 101.94(4) |
| [a]Metric parameters for **1** are reported according to the atom labeling scheme in Figure 1, which differs from prior structural report.[1] | | | |

**Table S3. Bond distances and angles of complex 2.**

| Atoms | Distance (Å) | Atoms | Angle (°) |
|---|---|---|---|
| Ni-N1 | 1.8528(8) | N1-Ni-N3 | 83.66(4) |
| Ni-N3 | 1.8580(8) | N1-Ni-S2 | 170.88(3) |
| Ni-S1 | 2.1617(3) | N3-Ni-S2 | 87.23(3) |
| Ni-S2 | 2.1576(2) | N1-Ni-S1 | 87.09(3) |
| S1-C5 | 1.7665(9) | S2-Ni-S1 | 102.019(10) |
| N1-C1 | 1.3038(11) | C5-S1-Ni | 94.59(3) |
| N1-N2 | 1.3694(11) | C1-N1-N2 | 119.80(8) |
| N2-C5 | 1.3222(12) | C1-N1-Ni | 115.46(6) |
| N5-C5 | 1.3456(12) | N2-N1-Ni | 124.64(6) |
| N5-C8 | 1.4453(13) | C5-N2-N1 | 110.47(8) |
| N5-C7 | 1.4570(13) | C5-N5-C8 | 124.17(9) |
| C1-C2 | 1.4658(13) | C5-N5-C7 | 118.67(8) |
| C1-C3 | 1.4857(13) | C8-N5-C7 | 117.15(8) |
| | | N1-C1-C2 | 112.75(8) |
| | | N1-C1-C3 | 123.71(9) |
| | | C2-C1-C3 | 123.52(8) |
| | | C1-C2-C4 | 122.36(8) |
| | | N2-C5-N5 | 116.74(8) |
| | | N2-C5-S1 | 123.18(7) |
| | | N5-C5-S1 | 120.06(7) |

**Table S4. Bond distances and angles of complex 3.**

| Atoms | Distance(Å) | Atoms | Angle(°) |
|---|---|---|---|
| Ni-N1 | 1.854(3) | N1-Ni-N3 | 83.65(13) |
| Ni-N3 | 1.863(3) | N1-Ni-S2 | 170.63(10) |
| Ni-S2 | 2.1527(10) | N3-Ni-S2 | 87.12(9) |
| Ni-S1 | 2.1542(11) | N1-Ni-S1 | 87.35(10) |
| S1-C5 | 1.763(4) | S2-Ni-S1 | 101.94(4) |
| N1-C1 | 1.310(5) | C5-S1-Ni | 94.17(13) |
| N1-N2 | 1.381(4) | C1-N1-N2 | 120.5(3) |
| N2-C5 | 1.308(5) | C1-N1-Ni | 115.3(2) |
| N5-C5 | 1.350(5) | N2-N1-Ni | 124.2(2) |
| N5-C7 | 1.440(5) | C5-N2-N1 | 109.8(3) |
| F1-C8 | 1.338(5) | C5-N5-C7 | 123.5(3) |
| F2-C8 | 1.339(4) | N1-C1-C2 | 112.6(3) |
| F3-C8 | 1.347(4) | N1-C1-C3 | 124.1(3) |
| C1-C2 | 1.474(5) | C2-C1-C3 | 123.3(3) |
| C1-C3 | 1.487(5) | C1-C2-C4 | 122.6(3) |
| | | N2-C5-N5 | 119.3(3) |
| | | N2-C5-S1 | 124.4(3) |
| | | N5-C5-S1 | 116.2(3) |
| | | N5-C7-C8 | 111.7(3) |
| | | F1-C8-F2 | 106.7(3) |
| | | F1-C8-F3 | 106.7(3) |
| | | F2-C8-F3 | 106.0(3) |
| | | F1-C8-C7 | 112.6(3) |
| | | F2-C8-C7 | 111.4(3) |
| | | F3-C8-C7 | 112.8(3) |

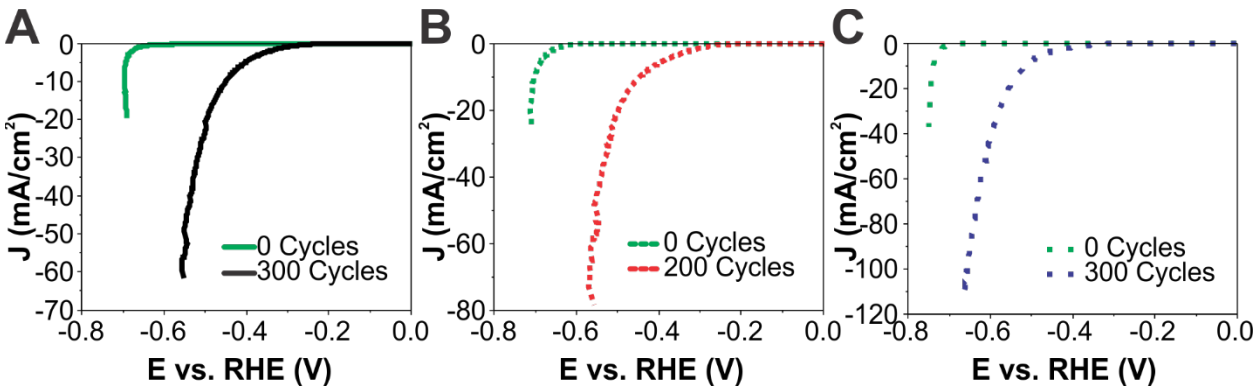


**Figure S6. Effects of reductive cycling from 0 to -0.8 V vs. RHE at 50 mV/s on the performance of the three modified electrodes. Vertical scale is expanded to show peak cathodic current for each electrode.**

(A) Polarization curves for GC-1 which exhibits peak HER performance after 300 cycles. (B) Polarization curves for GC-2 which exhibits peak HER performance after 200 cycles. (C) Polarization curves for GC-3 which exhibits peak HER performance after 300 cycles.

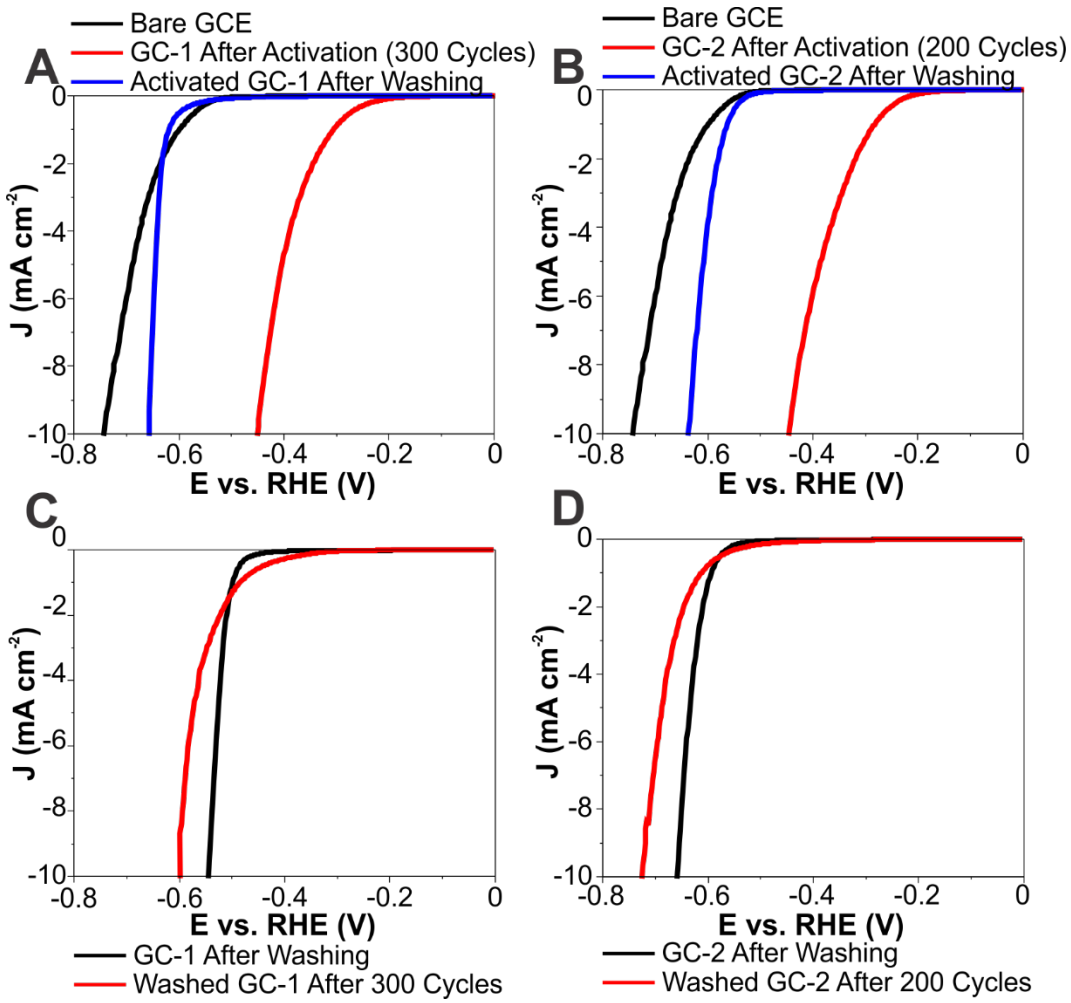


**Figure S7. Effect on HER performance of dipping modified electrodes in acetonitrile for 30 seconds at 800 RPM rotation.**

(A) **GC-1** conditioned to peak activity (300 cycles, red trace) and then washed in acetonitrile (blue trace) and compared to bare glassy carbon electrode (black trace). (B) **GC-2** conditioned to peak activity (200 cycles, red trace) and then washed in acetonitrile (blue trace) and compared to glassy carbon (black trace). (C) **GC-1** washed in acetonitrile before any conditioning (black trace) and subsequently conditioned to 300 cycles (red trace). (D) **GC-2** washed in acetonitrile before any conditioning (black trace) and subsequently conditioned to 200 cycles (red trace).

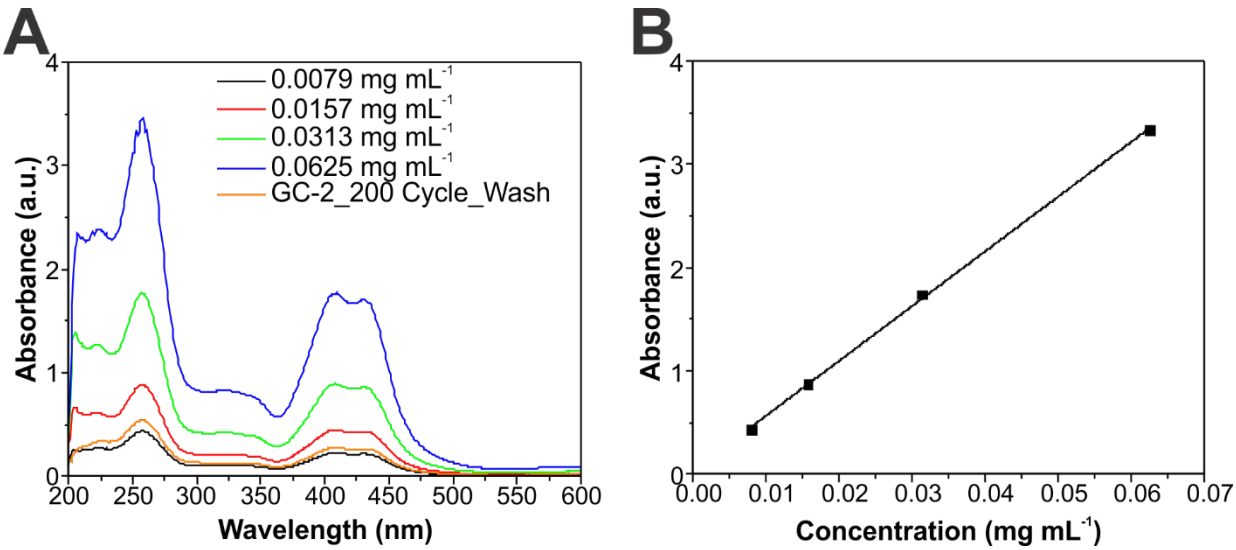


**Figure S8. UV-Visible Spectroscopy data for complex 2 in solution**

(A) UV-Vis spectra for complex **2** in acetonitrile solutions of known concentration and of unknown concentration after being washed off **GC-2** after conditioning to peak activity (200 cycles). (B) Calibration curve constructed from measured absorbances and known concentrations of standard acetonitrile solutions of **2**.

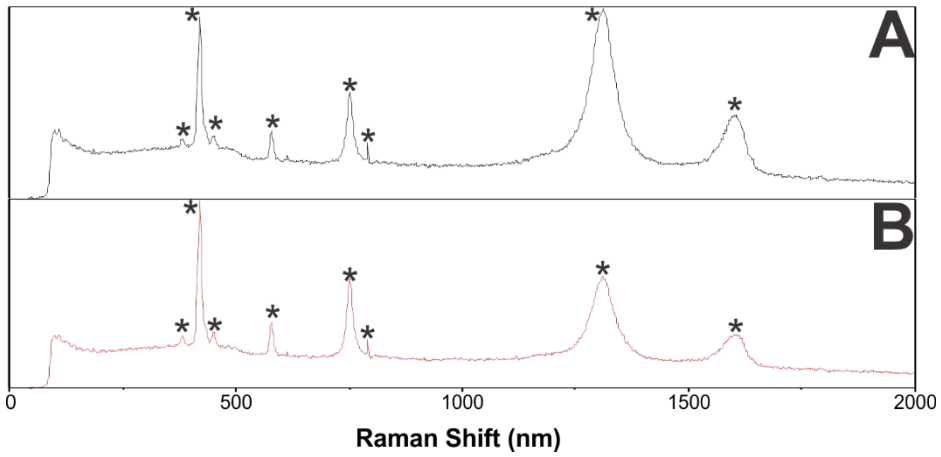


**Figure S9. Raman spectra of various electrodes and organic solutions with bands labelled.**

Raman spectrum of (A) Glassy carbon electrode with Nafion film. (B) Bare glassy carbon electrode. Peaks labelled with * are attributed to the glassy carbon electrode.

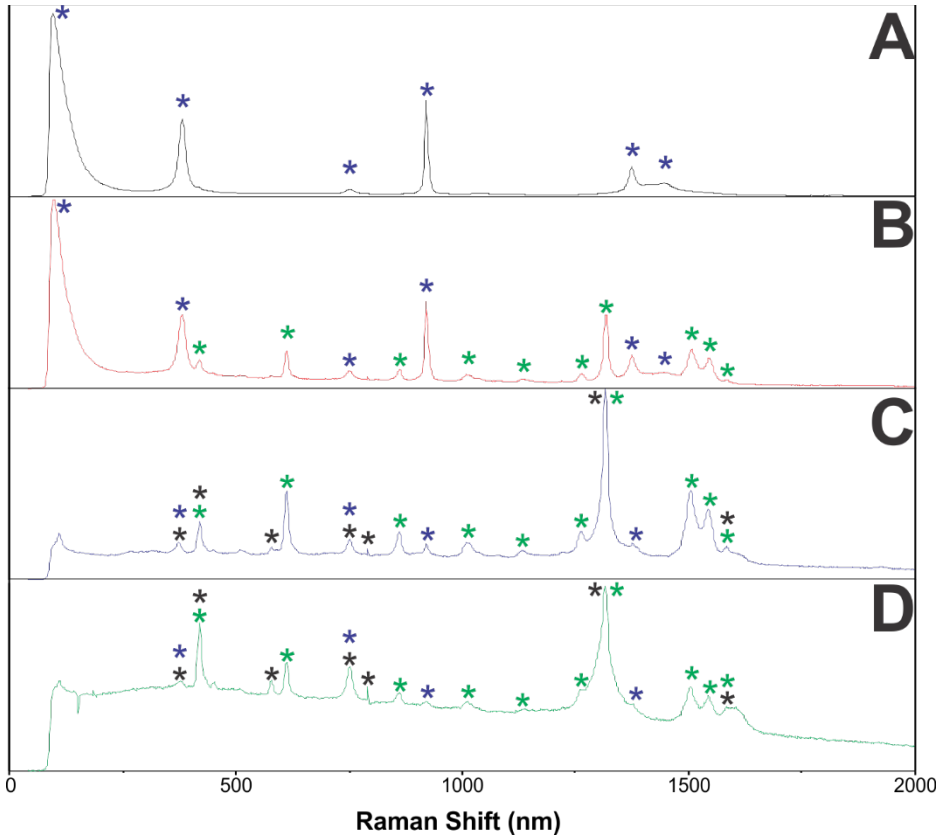


**Figure S10. Raman spectra of various electrodes and organic solutions with bands labelled.** Raman spectrum of (A) Acetonitrile. (B) Complex **2** in acetonitrile ink with Nafion. (C) **GC-2** as deposited. (D) **GC-2** after conditioning to peak activity (200 cycles). Peaks labelled with * are attributed to the glassy carbon electrode. Peaks labelled with * are attributed to acetonitrile. Peaks labelled with * are attributed to complex **2**.

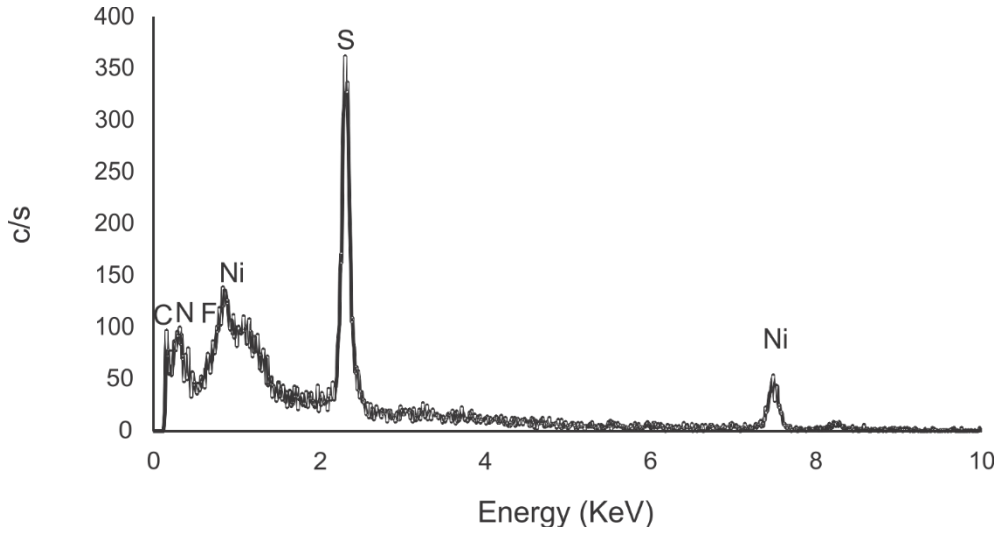


**Figure S11. EDS of GC-2 before reductive cycling.**

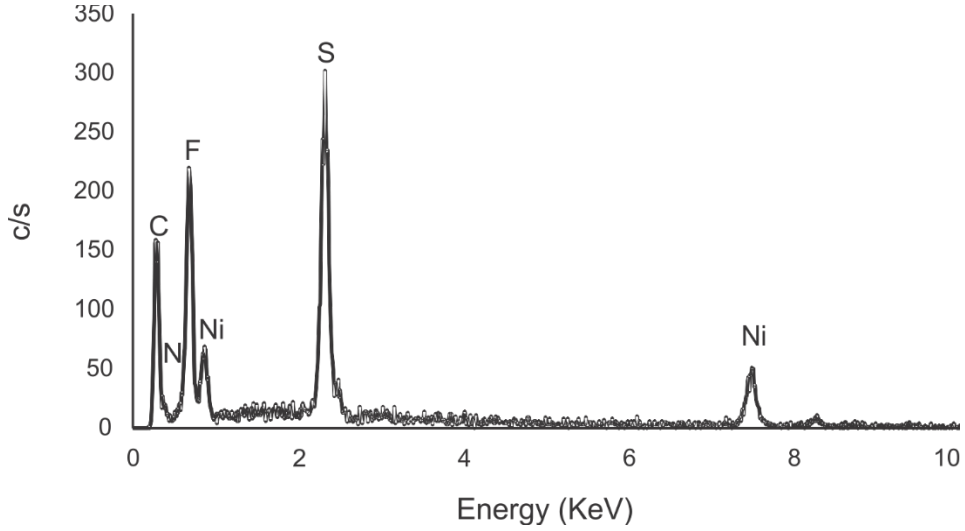


**Figure S12. EDS of GC-2 after 1000 cycles.**

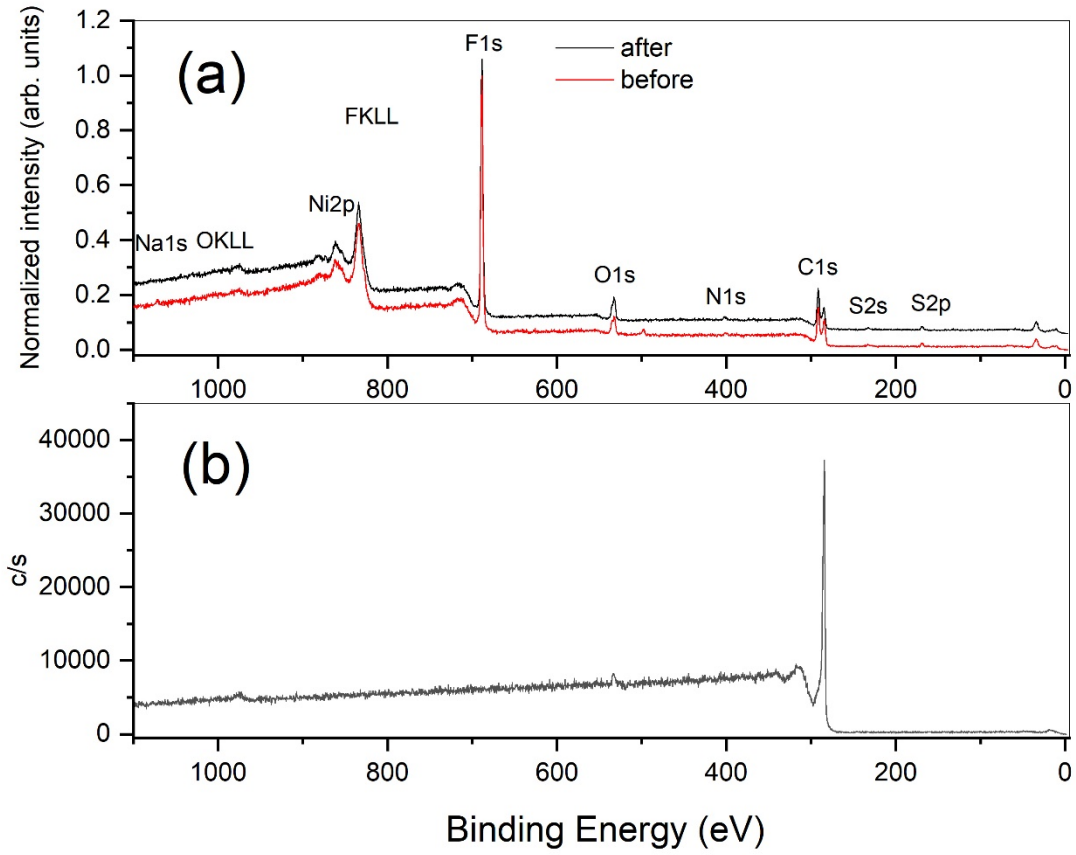


**Figure S13. Survey scans of the GC-2 electrode before (red) and after (black) conditioning to 1000 cycles (a) and of a pristine GCE (b).**

**Table S5. Atomic % of Ni2p, S2p and Ni1s before and after conditioning (1000 cycles).**

| | **N1s, at%** | **S2p, at%** | **Ni2p, at%** |
|---|---|---|---|
| **Before** | 61.3 | 26.74 | 11.96 |
| **After** | 66.74 | 23.35 | 9.91 |

**Table S6. XPS fitting parameters for nickel (Figure 8A).**

| Band | Pos | PosSep | B_FWHM | FWHM | Height | %Gauss | Area | %Area | ChiSquared |
|---|---|---|---|---|---|---|---|---|---|
| 1 | 853.38 | 0 | 3.12 | 3.12 | 1459 | 80 | 5309 | 37.12 | 1.94 |
| 2 | 859.24 | 5.86 | 6.72 | 6.72 | 482 | 80 | 3775 | 26.4 | |
| 3 | 870.81 | 17.43 | 3.37 | 3.37 | 675 | 80 | 2654 | 18.56 | |
| 4 | 876.33 | 22.95 | 6.39 | 6.39 | 344 | 80 | 2564 | 17.93 | |

**Table S7. XPS fitting parameters for sulfur (Figure 8B).**

| Band | Pos | PosSep | B_FWHM | FWHM | Height | %Gauss | Area | %Area | ChiSquared |
|---|---|---|---|---|---|---|---|---|---|
| 1 | 162.93 | 0 | 2.6 | 2.6 | 211 | 80 | 640 | 56.12 | 1.35 |
| 2 | 164.13 | 1.2 | 2.6 | 2.6 | 109 | 87 | 320 | 28.06 | |
| 3 | 168.33 | 5.4 | 2.7 | 2.7 | 37 | 70 | 120 | 10.54 | |
| 4 | 169.53 | 6.6 | 2.65 | 2.65 | 19 | 70 | 60 | 5.27 | |

**Table S8. XPS fitting parameters for nickel (Figure 10A).**

| Band | Pos | PosSep | B_FWHM | FWHM | Height | %Gauss | Area | %Area | ChiSquared |
|---|---|---|---|---|---|---|---|---|---|
| 1 | 853.31 | 0 | 2.84 | 2.84 | 6436 | 90 | 20406 | 29.53 | 2.81 |
| 2 | 858.1 | 4.79 | 8.79 | 8.79 | 2405 | 90 | 23572 | 34.11 | |
| 3 | 870.58 | 17.28 | 3.96 | 3.96 | 2656 | 90 | 11718 | 16.95 | |
| 4 | 876.2 | 22.89 | 8.94 | 8.94 | 1346 | 90 | 13417 | 19.41 | |

**Table S9. XPS fitting parameters for sulfur (Figure 10B).**

| Band | Pos | PosSep | B_FWHM | FWHM | Height | %Gauss | Area | %Area | ChiSquared |
|---|---|---|---|---|---|---|---|---|---|
| 1 | 162.32 | 0 | 2.57 | 2.57 | 1571 | 100 | 4293 | 51.15 | 1.71 |
| 2 | 163.52 | 1.2 | 2.57 | 2.57 | 718 | 80 | 2146 | 25.57 | |
| 3 | 164.48 | 2.16 | 3.2 | 3.2 | 221 | 60 | 895 | 10.66 | |
| 4 | 165.68 | 3.36 | 3.2 | 3.2 | 116 | 71 | 447 | 5.33 | |
| 5 | 168.22 | 5.9 | 2.7 | 2.7 | 124 | 70 | 408 | 4.86 | |
| 6 | 169.42 | 7.1 | 2.7 | 2.7 | 65 | 79 | 204 | 2.43 | |

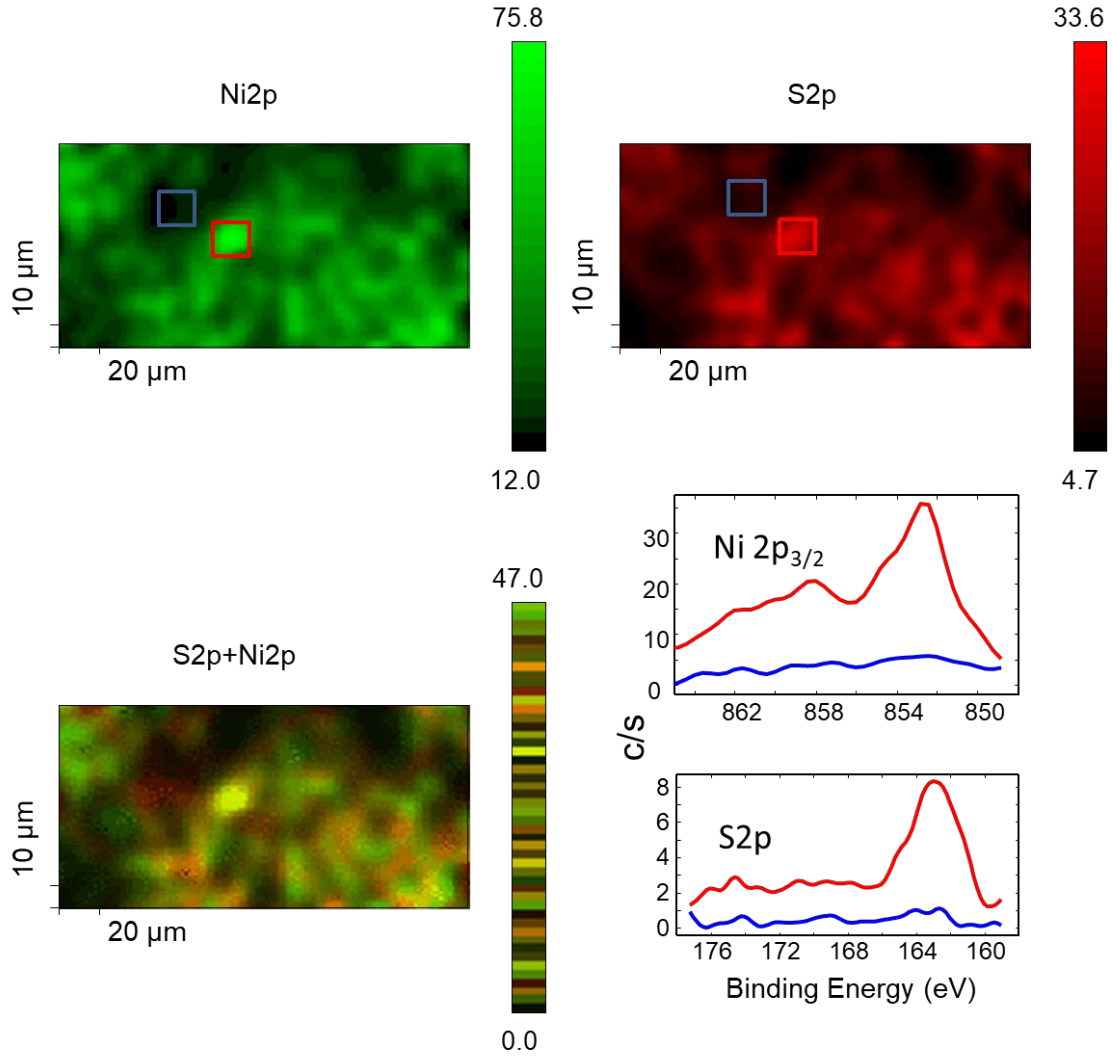


**Figure S14. Elemental mapping of nickel and sulfur.**

Elemental mapping of nickel (top left), sulfur (top right), and an overlay of both (bottom left) at 200 × 100 µm scanned area and XPS spectra (right bottom) in which the red trace and blue trace correspond to the pixels integrated through red and blue squares respectively.

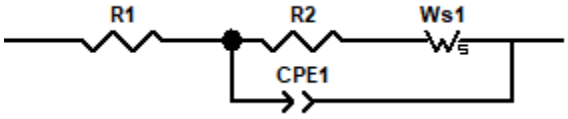


**Figure S15. Equivalent circuit model used to fit EIS data.**

**Table S10. Parameters obtained by fitting frequency response analysis (FRA) data to simulated RCW circuit.**

Zview software[2] was used to fit data. Q is the magnitude of the CPE, $R_c$ is the charge transfer resistance, $R_s$ is approximate solution resistance, n is the CPE exponent, and C is the capacitance. Capacitance values were calculated using $C = R_c^{\frac{1-n}{n}} * Q^{\frac{1}{n}}$.[3-7]

| **GC** | **1** | | | **2** | | | **3** | | |
|---|---|---|---|---|---|---|---|---|---|
| **# Cycles** | **0** | **300** | **1000** | **0** | **200** | **1000** | **0** | **300** | **1000** |
| **Q (F $s^{n-1}$)** | 2.43E-6 | 4.52E-6 | 4.46E-6 | 2.63E-6 | 6.10E-6 | 6.33E-6 | 3.55E-5 | 3.20E-5 | 5.14E-5 |
| **$R_c$ (Ω)** | 25099 | 270 | 374 | 18843 | 158 | 374 | 54764 | 631 | 1093 |
| **$R_s$ (Ω)** | 26.22 | 20.12 | 17.99 | 16.80 | 15.09 | 13.9 | 11.14 | 6.44 | 5.78 |
| **N** | 0.908 | 0.929 | 0.913 | 0.916 | 0.893 | 0.864 | 0.951 | 0.729 | 0.717 |
| **C (F)** | 1.83E-6 | 2.71E-6 | 2.43E-6 | 2.00E-6 | 2.65E-6 | 2.49E-6 | 3.67E-5 | 7.52E-6 | 1.66E-5 |
| $\chi^2$ | 0.00015 | 0.00121 | 0.00141 | 0.00072 | 0.00057 | 0.00057 | 0.03272 | 0.00163 | 0.00434 |

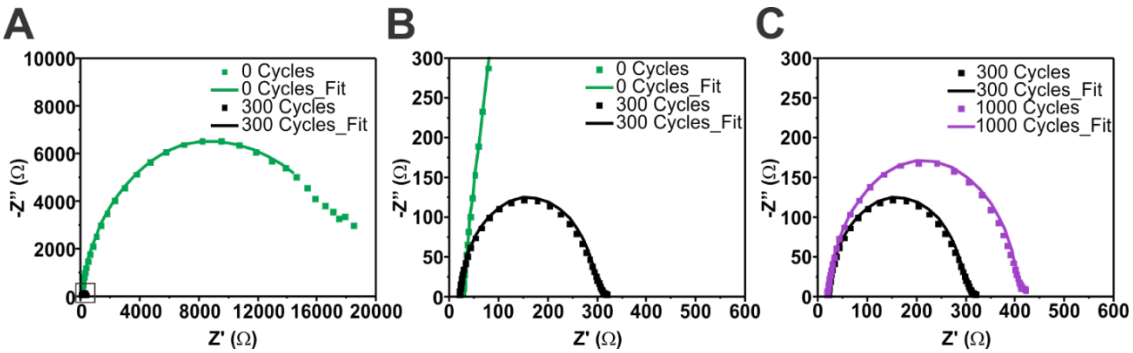


**Figure S16. Nyquist plots showing the effects of reductive cycling from 0 to -0.8 V vs. RHE at 50 mV/sec on the impedance of GC-1.**

Solid traces represent fitted impedance data, while dotted traces represent actual data. (A) Nyquist plot showing impedance at 0 cycles (before any reductive cycling) and after 300 cycles (peak activity, in small frame). (B) The same data as in (A), but with axes scaled down to show impedance after 300 cycles in greater detail. (C) Comparison of Nyquist plots for **GC-1** after 300 cycles and 1000 cycles.

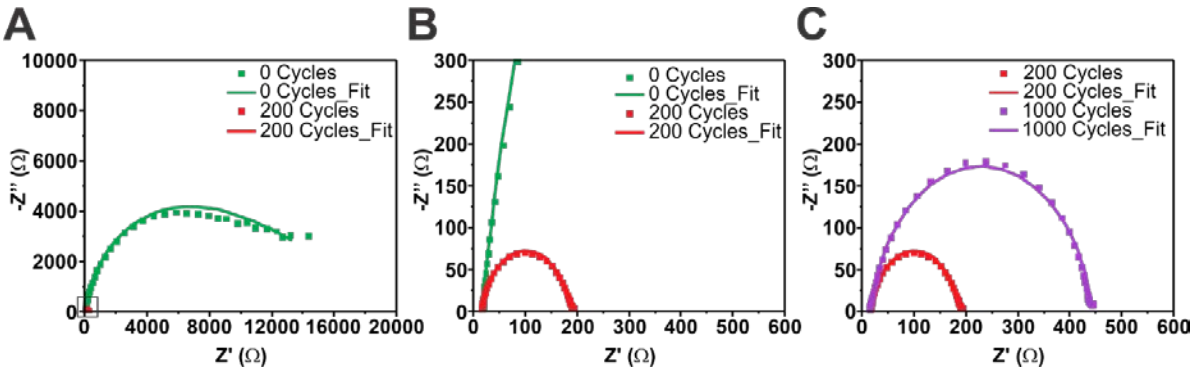


**Figure S17. Nyquist plots showing the effects of reductive cycling from 0 to -0.8 V vs. RHE at 50 mV/sec on the impedance of GC-2.**

Solid traces represent fitted impedance data, while dotted traces represent actual data. (A) Nyquist plot showing impedance at 0 cycles (before any reductive cycling) and after 200 cycles (peak activity, in small frame). (B) The same data as in (A), but with axes scaled down to show impedance after 200 cycles in greater detail. (C) Comparison of Nyquist plots for **GC-2** after 200 and 1000 cycles.

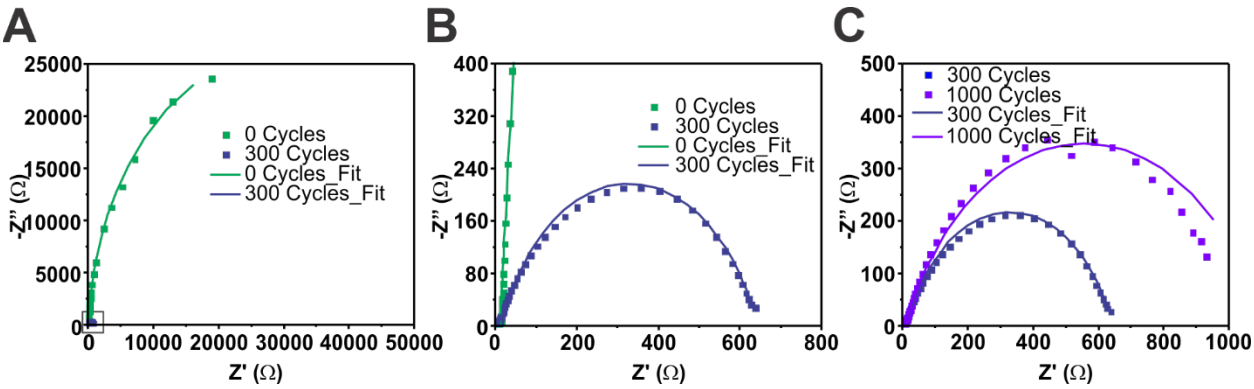


**Figure S18. Nyquist plots showing the effects of cycling from 0 to -0.8 V vs. RHE at 50 mV/sec on the impedance of GC-3**.

Solid traces represent fitted impedance data, while dotted traces represent actual data. (A) Nyquist plot showing impedance at 0 cycles (before any reductive cycling) and after 300 cycles (peak activity, in small frame). (B) The same data as in (A), but with axes scaled down to show impedance after 300 cycles in greater detail. (C) Comparison of Nyquist plots for **GC-3** after 300 and 1000 cycles.

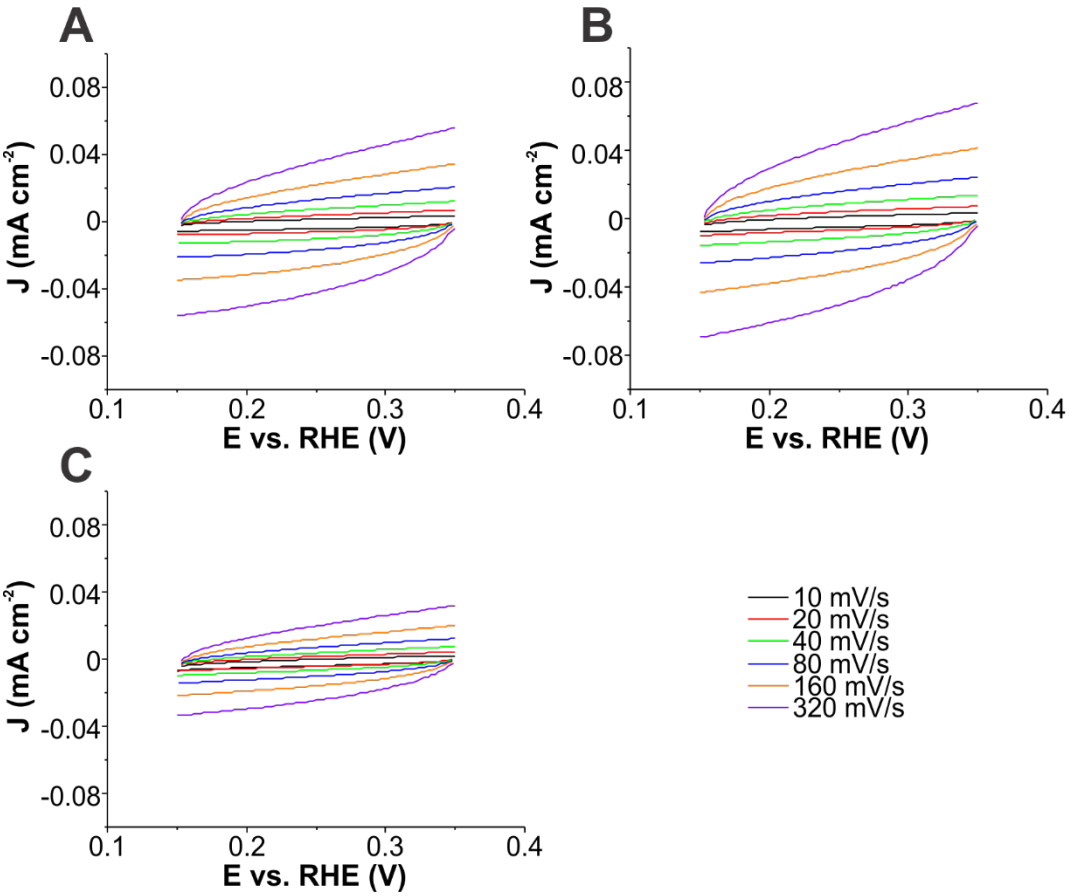


**Figure S19. Cyclic voltammetry plots showing the capacitive effects of varying scan speed over a non-Faradaic potential range for GC 1 – 3 as-deposited.**

(A) **GC-1** at 0 cycles. (B) **GC-2** at 0 cycles. (C) **GC-3** at 0 cycles

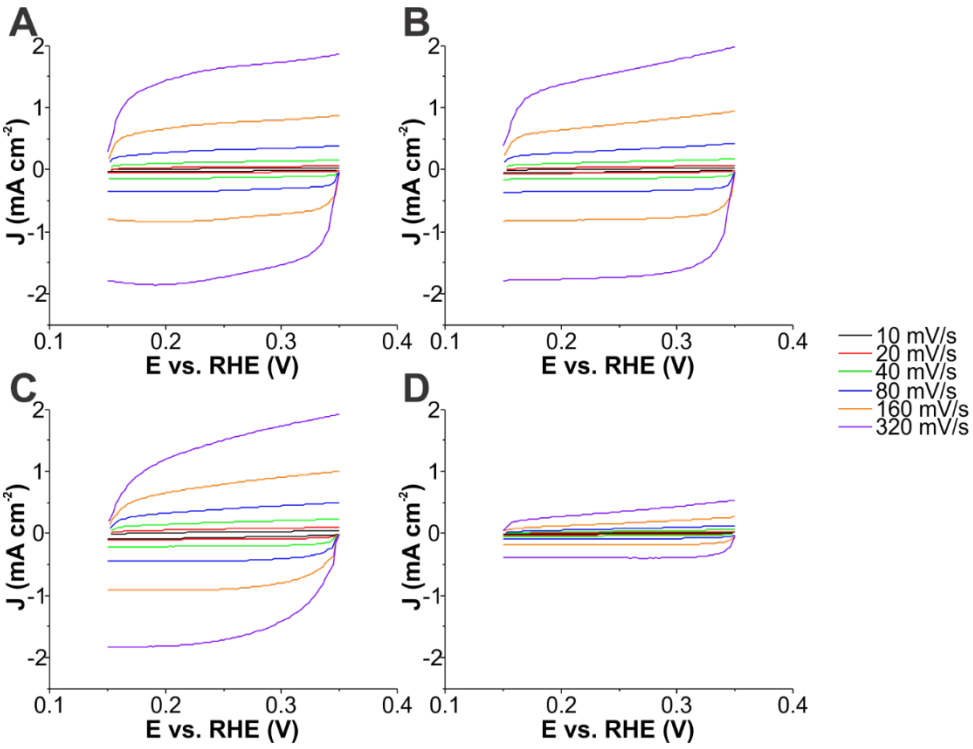


**Figure S20. Cyclic voltammetry plots showing the capacitive effects of varying scan speed over a non-Faradaic potential range for GC 1 – 3 after cycling to peak activity.**

(A) **GC-1** after 300 cycles. (B) **GC-2** after 200 cycles. (C) **GC-3** after 300 cycles. (D) Bare glassy carbon electrode.

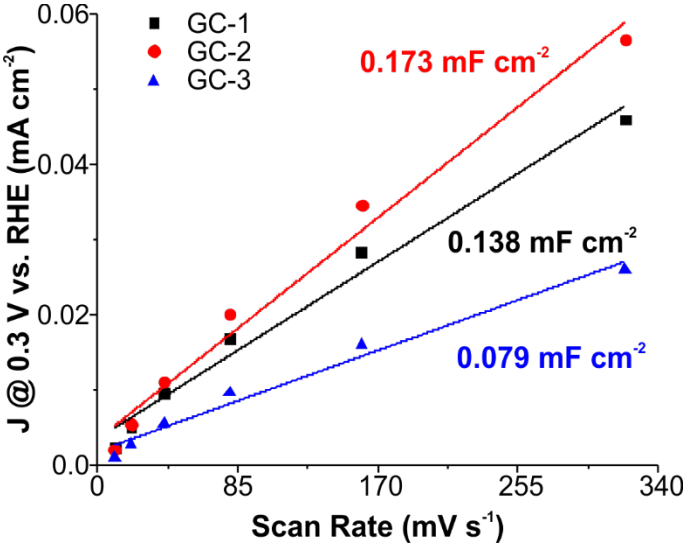


**Figure S21. Plot of average current density at 0.3 V vs. RHE as measured during anodic sweep as a function of scan rate for as-deposited electrodes.**

Slopes of the traces give the approximate capacitances of each modified electrode per unit geometric area (denoted in the same color as the corresponding trace).

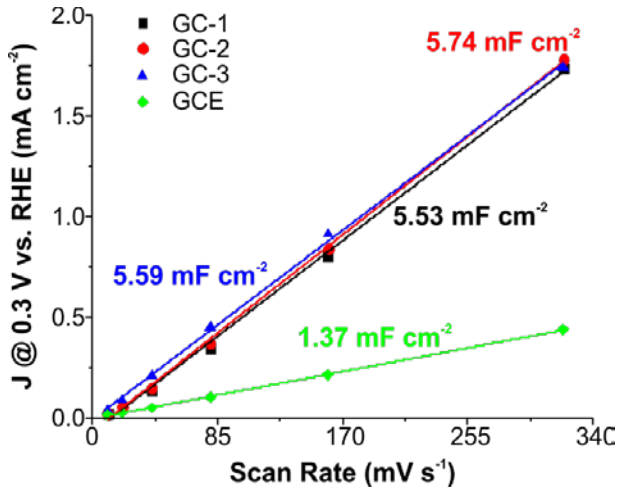


**Figure S22. Plot of average current density at 0.3 V vs. RHE as measured during anodic sweep as a function of scan rate for GC 1 – 3 after cycling to peak activity.**

Slopes of the traces give the approximate capacitances of each modified electrode per unit geometric area. The black trace corresponds to **GC-1** after 300 cycles, the red trace corresponds to **GC-2** after 200 cycles, and the blue trace corresponds to **GC-3** after 300 cycles.

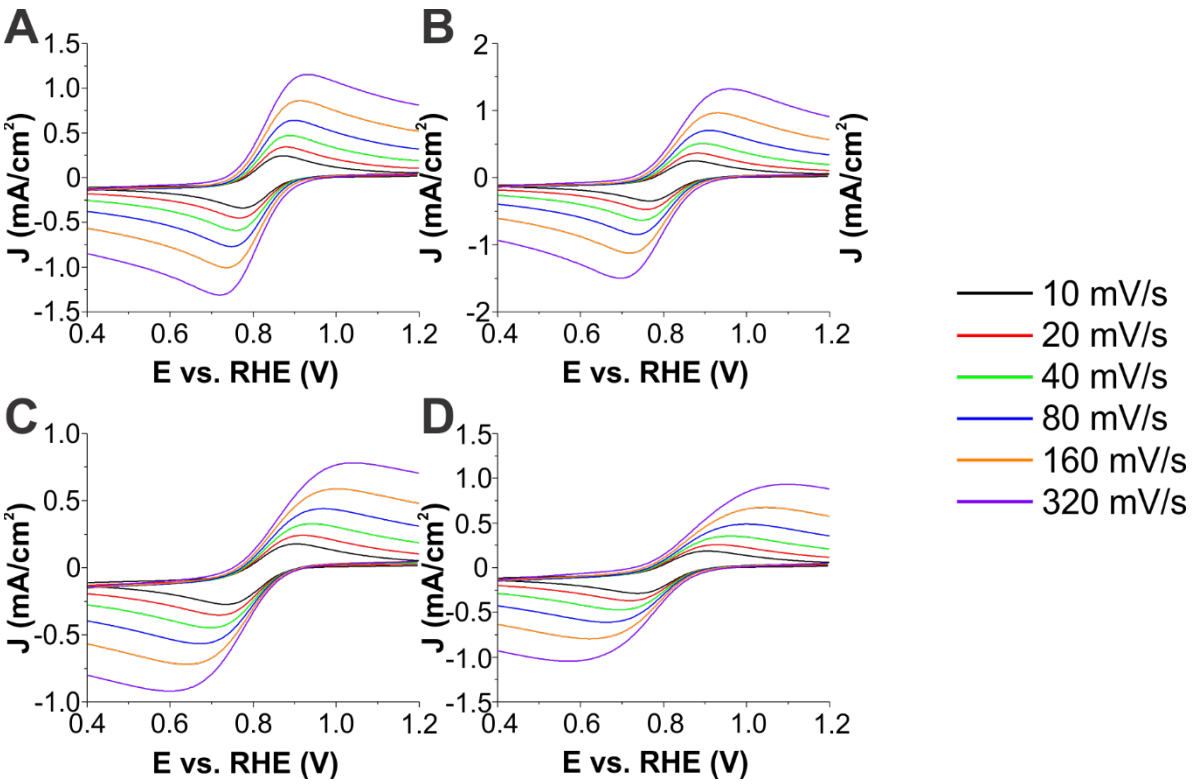


**Figure S23. Oxidation (top peak) and reduction (bottom peak) of ferricyanide redox couple at 5 mM in 0.1 M potassium nitrate solution.**

(A) **GC-1** as-deposited. (B) **GC-1** after conditioning to 300 cycles. (C) **GC-2** as-deposited. (D) **GC-2** after conditioning to 200 cycles.

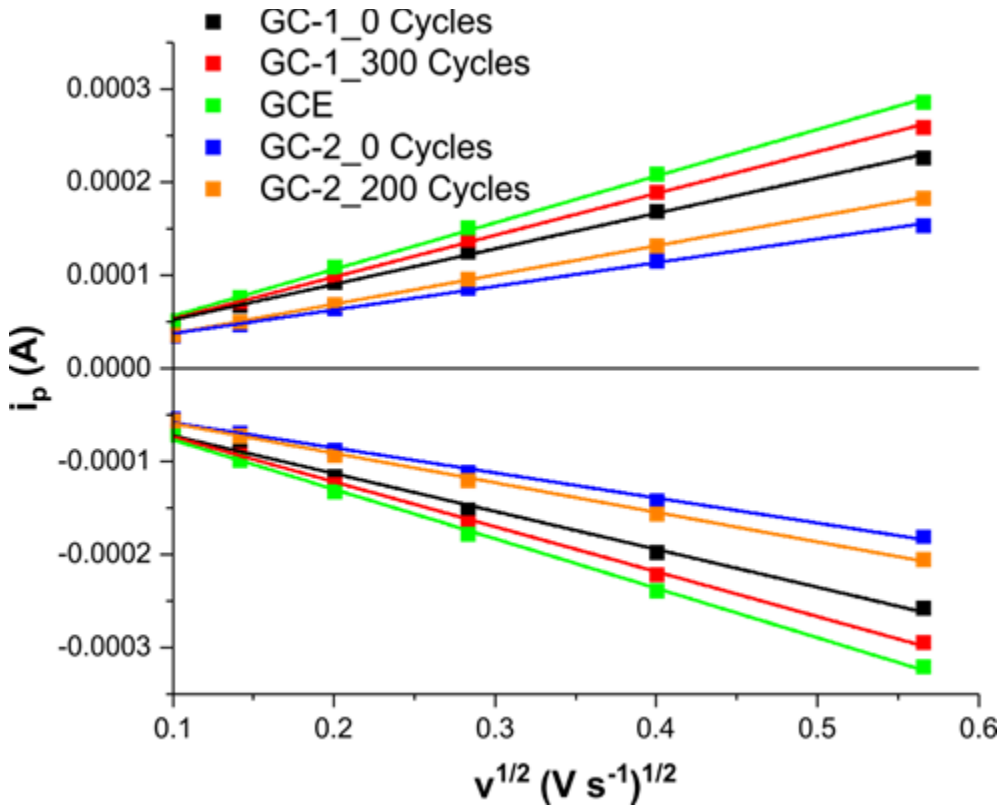


**Figure S24. Plot of maximum current (top, for anodic sweeps) and minimum current (bottom, for cathodic sweeps) associated with ferricyanide reduction/oxidation cyclic voltammetry experiment as a function of the square root of scan rate.**

**Table S11. Slopes of the traces of maximum/minimum current densities as a function of the square root of scan rate for ferricyanide oxidation/reduction experiments as well as areas calculated from the Randles-Sevcik equation.**

| | **Anodic** | | **Cathodic** | |
|---|---|---|---|---|
| **Material** | **Slope** | **Area ($cm^2$)** | **Slope** | **Area ($cm^2$)** |
| **GC-1_300 Cycles** | $4.5x10^{-4}$ | 0.12 | $-4.8x10^{-4}$ | 0.14 |
| **GC-1_0 Cycles** | $3.8x10^{-4}$ | 0.11 | $-4.1x10^{-4}$ | 0.12 |
| **GC-2_200 Cycles** | $3.1x10^{-4}$ | 0.09 | $-3.2x10^{-4}$ | 0.09 |
| **GC-2_0 Cycles** | $2.5x10^{-4}$ | 0.07 | $-2.7x10^{-4}$ | 0.08 |

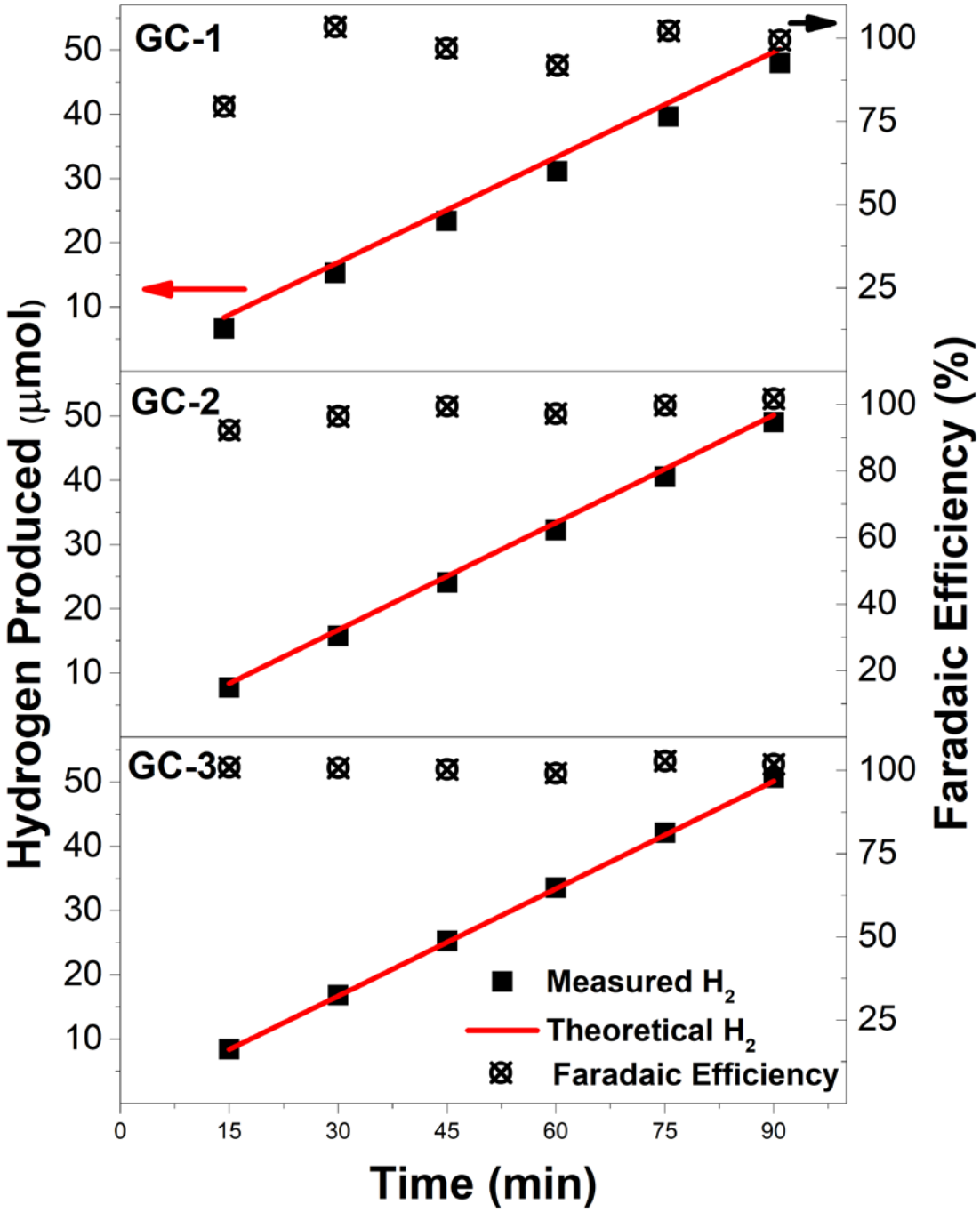


**Figure S25. Plot of theoretical hydrogen, measured hydrogen, and Faradaic efficiencies for GC 1 – 3 after cycling to peak activity.**

Theoretical $H_2$ is calculated from the coulombs of charge passed during the experiment. Measured $H_2$ was detected via gas chromatography. The Faradaic efficiency was calculating by comparing these two values. **GC 1 – 3** were evaluated after 300, 200, and 300 cycles respectively.

**References**


1. Blower, P. J.; Castle, T. C.; Cowley, A. R.; Dilworth, J. R.; Donnelly, P. S.; Labisbal, E.; Sowrey, F. E.; Teat, S. J.; Went, M. J. Structural trends in copper(II) bis(thiosemicarbazone) radiopharmaceuticals. *Dalton Trans.* **2003**, 4416-4425
2. Johnson, D. ZView: a software program for IES analysis, Version 2.8, Scribner Associates. *Inc., Southern Pines, NC* **2002**, 200
3. Chinarro, E.; Jurado, J.; Figueiredo, F.; Frade, J. Bulk and grain boundary conductivity of $Ca_{0.97}Ti_{1-x}Fe_xO_{3-\delta}$ materials. *Solid State Ionics* **2003**, 160, 161-168
4. Gore, C. M.; White, J. O.; Wachsman, E. D.; Thangadurai, V. Effect of composition and microstructure on electrical properties and $CO_2$ stability of donor-doped, proton conducting $BaCe_{1-(x+y)}Zr_xNb_yO_3$. *J. Mater. Chem. A* **2014**, 2, 2363-2373
5. Li, Q.; Thangadurai, V. Synthesis, structure and electrical properties of Mo-doped $CeO_2$– materials for SOFCs. *Fuel Cells* **2009**, 9, 684-698
6. Li, Q.; Thangadurai, V. A comparative 2 and 4-probe DC and 2-probe AC electrical conductivity of novel co-doped $Ce_{0.9-x}RE_xMo_{0.1}O_{2.1-0.5x}$ (RE = Y, Sm, Gd; x = 0.2, 0.3). *J. Mater. Chem.* **2010**, 20, 7970-7983
7. Hjalmarsson, P.; Søgaard, M.; Mogensen, M. Electrochemical behaviour of $(La_{1-x}Sr_x)_sCo_{1-y}Ni_yO_{3-\delta}$ as porous SOFC cathodes. *Solid State Ionics* **2009**, 180, 1395-1405